3 Objective Quantitative Evaluation of Angle Closure

Yu Meng Wang and Carol Y. Cheung

Abstract

Several limitations have been encountered with the reference standard of gonioscopy for angle assessment. Advancements in ophthalmic imaging technologies, especially anterior segment optical coherence tomography (AS-OCT) in recent years, have established robust, reliable, and quantitative protocols to examine the structure of the anterior segment with proven usefulness to detect various ocular complications including angle closure. The goal of this chapter is to review the basics of the most commonly used anterior segment imaging techniques (ultrasound biomicroscopy and AS-OCT), including a concise update of how they work and how objective and quantitative evaluation can be conducted in clinical practice.

Keywords

Angle closure · Anterior segment OCT · Anterior segment

3.1 Introduction

Angle closure diseases can be classified into different subtypes including primary angle closure suspect (PACS), acute angle closure (AAC), and primary angle closure glaucoma (PACG) [1]. Among them, PACG is potentially blinding, and so far, with no cure. Control of intraocular pressure (IOP) helps inhibition of disease progression in some patients. These subtypes can also represent different stages of disease severities. Individuals who are PACS can advance to AAC, and further to PACG, which is potentially blinding. The advancements are affected by both inductive and constitutive risk factors, while some patients remain stable in their ocular conditions. Several ocular risk factors have been identified for angle closure disease. These include short axial length, shallow anterior chamber (AC), thick peripheral iris roll (PIR), and thick and anteriorly positioned lens [2]. Qualitative and quantitative evaluation of the anterior segment in these eyes are helpful in understanding the pathogenesis of angle closure [3], and thus can provide clues to further disease development. Consequentially, prediction may be possible.

Traditional approaches, such as UBM, for anterior chamber angle (ACA) imaging mostly work on obtaining a single cross-sectional slice view across the anterior segment Furthermore, quantitative analysis of these images requires expertise to conduct the analysis. Interpretations

Y. M. Wang · C. Y. Cheung (✉)
Department of Ophthalmology and Visual Sciences, The Chinese University of Hong Kong, Hong Kong, China
e-mail: carolcheung@cuhk.edu.hk

C. C. Y. Tham (ed.), *Primary Angle Closure Glaucoma (PACG)*,
https://doi.org/10.1007/978-981-15-8120-5_3

of the results also need personal experiences and evaluations which, inevitably, can be subjective. Advances in imaging technologies and software in recent years have enhanced the robustness of anterior segment imaging and its quantitative measurement. Newer approaches using swept-source optical coherence tomography (SS-OCT) allow for imaging of the entire ACA over 360 degree and provide a summary measure of the extent of angle closure [4]. Data collection, analysis, and interpretation are aided by high-performance software to obtain objective and quantitative measurements. These modern imaging technologies are expected to be very effectively applied for evaluation of angle closure, especially in long-term management and assessment of disease development [5].

In this chapter, we review the basics of the most commonly used anterior segment imaging techniques (ultrasound biomicroscopy and AS-OCT), including a concise update of how they work and how objective and quantitative evaluation can be conducted in clinical practice.

3.2 Qualitative and Quantitative Evaluation Approaches of the Anterior Segment

3.2.1 Ultrasound Biomicroscopy

Ultrasound Biomicroscopy (UBM) provides highly resolved, reliable, and repeatable images of the anterior segment (Fig. 3.1). Software are available for quantitative measurements, such as ACA, angle opening distance (AOD) and angle recess area (ARA). UBM uses high-frequency ultrasound at 50–100 MHz for anterior segment imaging. A computer program then converts these sound waves into a high-resolution B-scan image. The probe provides a scan rate of 8 Hz and enables a lateral resolution of 50 μm and an axial resolution of 25 μm [6, 7]. UBM has previously been shown to have a good agreement with gonioscopy in its ability to evaluate angle closure when performed in a darkened room [8]. In addition, unlike conventional methodologies of AS-OCT, UBM can achieve visualization of structures posterior to the iris pigment epithelium [6, 7, 9, 10] as sound penetrates the pigment epithelium but light does not. Thus, UBM is capable for visualizing fine details of the posterior chamber structures, including the lens zonules, ciliary body, and even the anterior choroid. Unlike AS-OCT, UBM can also be performed with the subject lying down, and thus it is useful in the operating room when examination is needed for the patient under anesthesia. However, UBM is an eye contact method and requires highly skilled technicians or doctors to operate Table 3.1 highlights the main differences between AS-OCT and UBM. It is noted that prior studies have reported excellent intra-observer reproducibility but poor inter-observer repro-

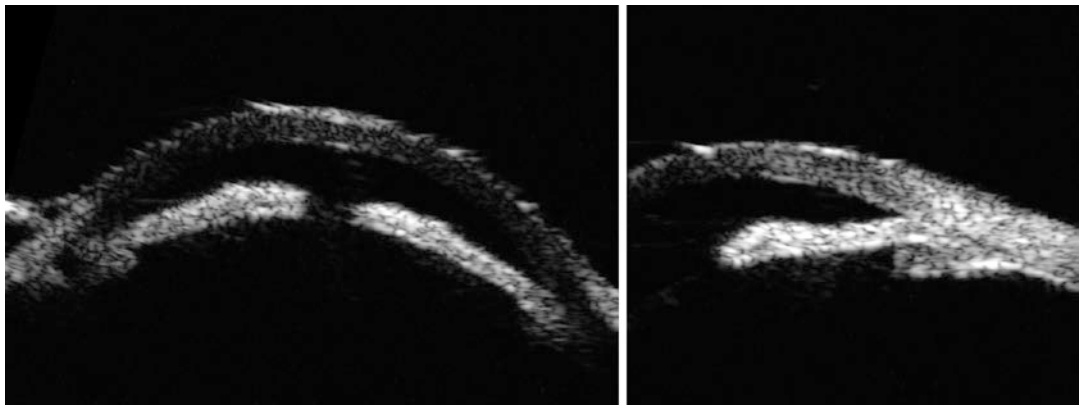

Fig. 3.1 Anterior chamber and its angle imaged by UBM

ducibility in assessing the ACA or iris dimensions measured from UBM images [11, 12]. In addition, UBM may have a narrower field of view compared to the AS-OCT [13–15].

Table 3.1 Comparison of UBM and AS-OCT in anterior segment imaging

UBM	AS-OCT
Require contact and a liquid coupling medium	Noncontact
Mild patient discomfort	No patient discomfort apart from some patience is required during the measurement
Skilled operator requiring experience	Non-skilled operator can be readily trained
Lower axial resolution	High axial resolution
Capable to visualize structures posterior to the iris pigment epithelium	Limited ability to visualize structures posterior to the iris pigment epithelium
Slower acquisition time	Fast acquisition time
Smaller field of view	Wide field of view
Seated upright or supine positions	Seated upright position
Can image through opaque corneas	Use for clear corneas

AS-OCT Anterior segment optical coherence tomography, *UBM* Ultrasound biomicroscopy

3.2.2 Anterior Segment Optical Coherence Tomography

Anterior Segment Optical Coherence Tomography (AS-OCT) is a non-contact and rapid imaging device that uses low-coherence interferometry to obtain cross-sectional images of the anterior segment [16]. Figure 3.2 shows the structure of anterior segment imaged by AS-OCT. Studies have shown that measurements from the cross-sectional AS-OCT images, such as anterior chamber depth (ACD), anterior chamber area, AOD, trabecular iris space area (TISA), and iris thickness, are with good reproducibility [17, 18]. Unlike gonioscopy, the measurement is objective and not operator dependent. There are advanced models of AS-OCT based on different configurations, including time-domain (TD-OCT), spectral-domain (SD-OCT), and swept-source (SS-OCT) [19]. Table 3.2 summarizes the features of each of these configurations. Imaging based on SS-OCT and SD-OCT are considered a type of Fourier-domain (FD) OCT. Compared with TD-OCT, the inherent signal-to-noise ratio is lower and the imaging speed (up to 20–40 kHz line-scan rate) of FD-based OCT is higher.

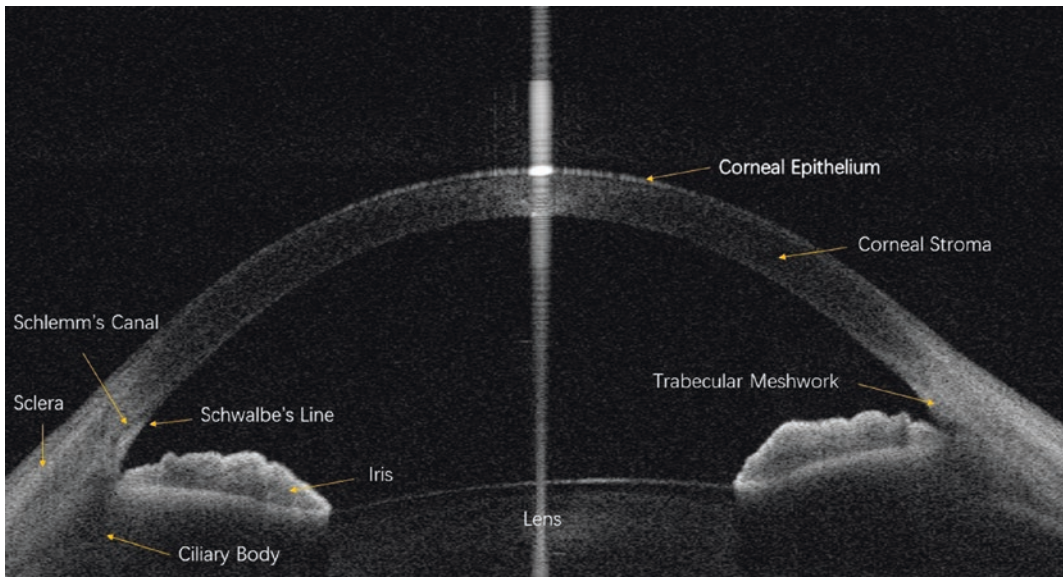

Fig. 3.2 Structure of anterior segment imaged by AS-OCT

Table 3.2 Comparison of different modes of AS-OCT

	Time-domain AS-OCT	Posterior segment spectral-domain OCT	Swept-source AS-OCT
Types	Zeiss Visante, Heidelberg SL-OCT	Spectralis OCT, Cirrus HDOCT, Optovue OCT	Casia SS-1000 OCT Casia2
Central wavelength	1310 nm	880 nm (Spectralis) 840 nm (Cirrus & Optovue)	1310 nm
Axial resolution	>15 μm	<5 μm	10 μm
Imaging depth range	6–7 mm	2–3 mm	6 mm
Line-scan rate	2 kHz/200 HZ	20–40 kHz	30 kHz

AS-OCT Anterior segment optical coherence tomography, *SL-OCT* Slit-lamp optical coherence tomography

With the advent of AS-OCT, imaging researchers can capture the entire cross-section of the anterior segment in a single high-resolution image to enable precise assessment of lens, in addition to the angle and iris parameters. Lens vault (LV), defined as the perpendicular distance between the anterior lens pole and the horizontal line joining the temporal and nasal scleral spurs (SSs), is a structural parameter associated with angle closure that can be measured with AS-OCT [20, 21]. There are reported patients with exaggerated LV in which the iris appeared to drape the anterior surface of the lens, giving rise to a "volcano-like configuration" without an increase in iris curvature (I-curve) [17]. As the I-curve has been reported to be only moderately correlated with increased LV, pupil block may not be the only mechanism by which increased LV causes angle closure [22].

Shabana et al. assessed four different mechanisms of primary angle closure (PAC) by evaluating AS-OCT images: pupil block, plateau iris configuration, thick peripheral iris roll (PIR), and exaggerated LV. They reported significant differences in quantitative angle closure parameters for these different PAC mechanisms. This classification scheme may be effective for the evaluation of progression of individuals with angle closure into angle diseases [17].

3.2.2.1 Posterior Segment Spectral-Domain OCT

With the use of an external adaptor lens, posterior segment Segment Spectral-Domain OCT (SD-OCT) such as Spectralis OCT, Cirrus HDOCT, and Optovue OCT, is also possible to image the anterior chamber of an eye [23–25]. The Spectralis uses shorter 880 nm wavelength light to produce higher axial-resolution images, which permits visualization of intraocular structures such as Schwalbe's line and Schlemm's canal [26, 27]. However, the shorter wavelength also results in a shorter imaging range, thus precluding visualization of the entire anterior chamber in a single scan. Previous study identified good intra-device reproducibility and good inter-device agreement of anterior segment parameter measurement values for the CASIA2 and Spectralis OCT2 [25].

3.2.2.2 Swept-Source OCT

Swept-Source OCT (SS-OCT) is the latest generation of OCT and is currently commercially available. It utilizes a swept-source laser wavelength of 1310 nm based on FD technology and employing a scan speed of 30,000 A-scans/second and an axial resolution of 10 μm. Such capabilities enable capturing images of extremely high resolution. One commonly used model is the Casia SS-1000 OCT (Tomey, Nagoya, Japan). Less than 3 seconds are needed to image the angle morphology in high-resolution and circumferentially 360°. Examples of eyes with open angle and closed angle were shown in Figs. 3.3, 3.4, 3.5 and 3.6.

3.2.2.3 Comparison Between UBM and AS-OCT

Compared with UBM, AS-OCT achieves better resolution and does not require contact with the

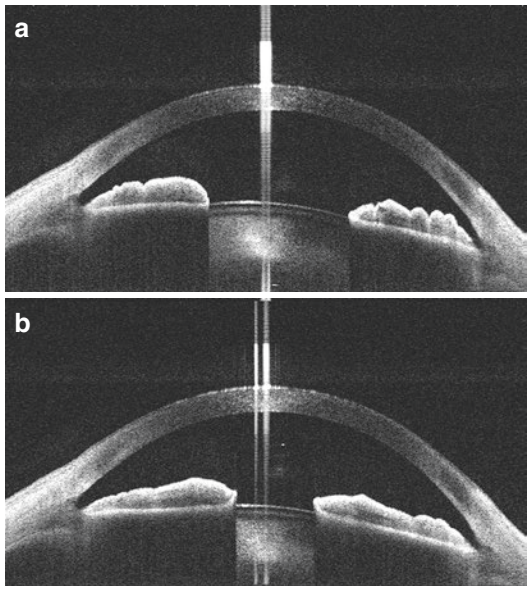

Fig. 3.3 Example of open angle in cross-sectional view: (**a**) imaged in dark condition; (**b**) Imaged in lighting condition

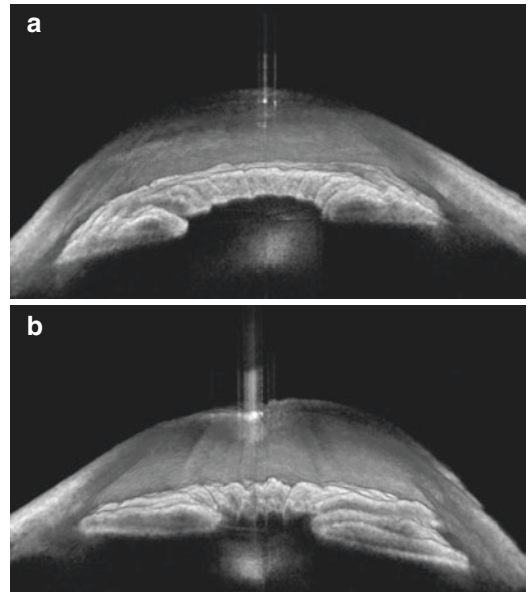

Fig. 3.5 Example of open angle in 3D view: (**a**) imaged in dark condition; (**b**) imaged in lighting condition

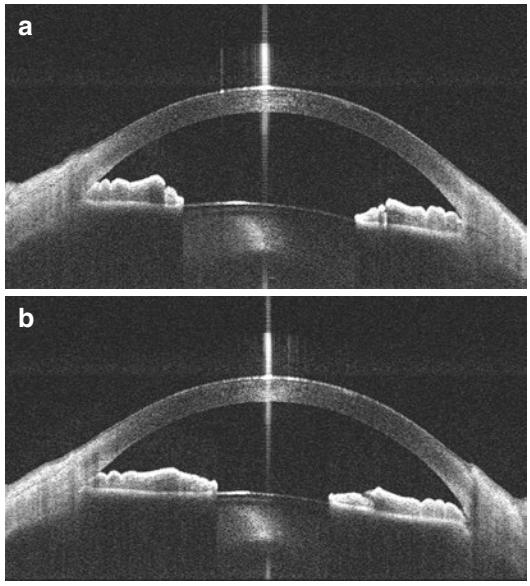

Fig. 3.4 Example of closed angle in cross-sectional view: (**a**) imaged in dark; (**b**) imaged in lighting condition

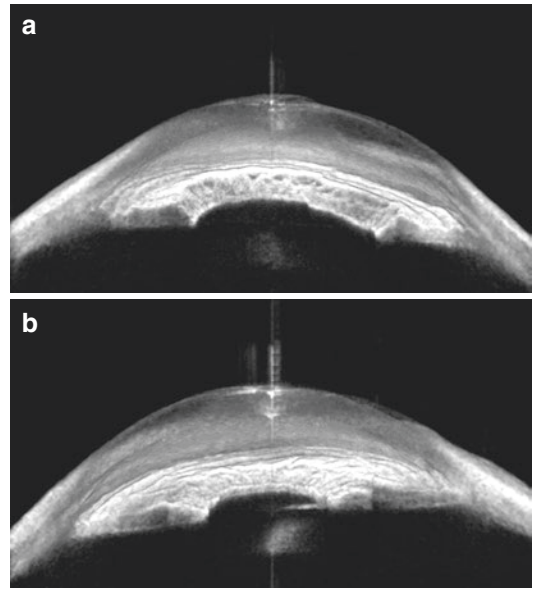

Fig. 3.6 Example of closed angle in 3D view: (**a**) imaged in dark condition; (**b**) imaged in lighting condition

ocular surface [28]. The main limitation of AS-OCT is that the light energy cannot penetrate tissues behind the iris pigment epithelium. Consequently, AS-OCT cannot visualize any structures posterior to the iris pigment epithelium. Thus, AS-OCT is not useful in the detection of ocular complications such as plateau iris syndrome and phacomorphic angle-closure (Table 3.1).

3.3 Quantitative Metrics of Angle Closure

3.3.1 Quantitative Metrics in 2D AS-OCT Images

Biometric analysis of the ACA requires a reference landmark from which the angle measurements are derived. Typically, the scleral spur (SS) (Fig. 3.7) is used as a reference point for structural measurements of AOD, [9] TISA, ARA, [29] scleral thickness, [11] trabecular meshwork-ciliary process distance, and [11] trabecular iris angle (TIA) [9, 15] (Fig. 3.8). Other biometric parameters that can be measured by the AS-OCT include iris thickness, iris curvature, AC depth, AC width, and lens vault [30]. These parameters are further described in Table 3.3. Although these AS-OCT parameters, including ACD and ACA, [22] have been shown to differ in various subtypes of angle closure disease, characteristic features that may predict development to PACG from eyes with narrow angles have not yet been established.

Manual identification of the SS prior to measurements is important to the accuracy of the measurements of various biometric parameters. But there are disadvantages in the use of SS as an anchor for high-resolution imaging [11]. There is currently no technology available that can automatically identify the SS. Difficulty in identifying the SS as a reference point has been cited in numerous studies, with reportedly 15–28% of AS-OCT images not able to identify the SS [31, 32]. So far, there is no consensus regarding the relationships between various AS-OCT obtained

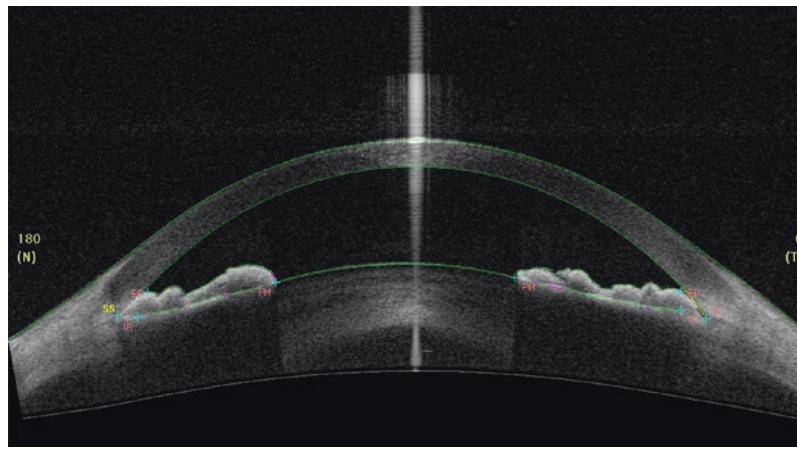

Fig. 3.7 Landmarks of anterior segment structure for quantitative measurement of ACA: Scleral Spur (SS), ITC End Point (EP), and Iris Root (IR)

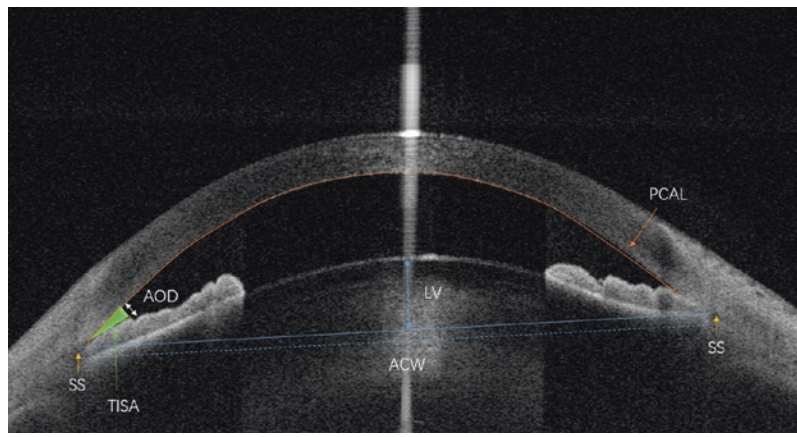

Fig. 3.8 Measurement of anterior segment parameters on a cross-sectional anterior segment optical coherence tomography image. *ACW* anterior chamber width, *AOD* anterior opening distance, *SS* scleral spur, *LV* lens vault, *PCAL* posterior corneal arc length, *TISA* trabecular iris space area

Table 3.3 Definitions of quantitative AS-OCT biometric parameters

Parameter	Group	Abbreviation	Unit	Description
Angle opening distance	ACA related	AOD	μm	Linear distance between the point of the inner corneoscleral wall and the iris
Angle recess area	ACA related	ARA	μm^2	The triangular area demarcated by the anterior iris surface, corneal endothelium, and a line perpendicular to the corneal endothelium drawn from a point 750 μm anterior to the scleral spur to the iris surface
Trabecular iris angle	ACA related	TIA	Degree	Angle formed from angle recess to points 500 μm from scleral spur on trabecular meshwork and perpendicular on surface of iris
Trabecular iris space area	ACA related	TISA	mm^2	A trapezoidal area measuring the filtering area. The defining boundaries for this trapezoidal area are: Anteriorly, the AOD; posteriorly, a line drawn from the scleral spur perpendicular to the plane of the inner scleral wall to the opposing iris; superiorly, the inner corneoscleral wall; and inferiorly, the iris surface
Iris thickness	Iris related	IT	mm	Measured from a perpendicular point 500 μm or 750 μm from the scleral spur, with the scleral spur defined as the point at which a change in the curvature of the inner surface of the angle is apparent
Iris cross-sectional area	Iris related	IA	mm^2	The average of the cross-sectional area of both nasal and temporal and nasal sides
Iris curvature	Iris related	IC	mm	Maximum perpendicular distance between iris pigment epithelium and line, connecting the most peripheral to most central point of the epithelium
Iris–trabecular contact index	Iris related	ITC index	NA	The ITC index was calculated as a percentage of the angle that was closed on SSOCT images. The ITC graph with the *Y*-axis representing ITC and the *X*-axis representing the degree of the angle. The graph above the red horizontal line demonstrates the amount of angle closure measured as the ITC index in percentage
Anterior chamber depth	AC related	ACD	mm	Distance from corneal endothelium to anterior surface of the lens
Anterior chamber width	AC related	ACW	mm	Distance of a horizontal line joining the two scleral spurs
Anterior chamber volume	AC related	ACV	mm^3	The volume of anterior chamber
Lens vault	Lens related	LV	mm	Perpendicular distance between anterior pole of the crystalline lens and the horizontal line joining the two scleral spurs
Scleral thickness	NA	ST	mm	Measured perpendicular from the scleral spur to the episcleral surface

AS-OCT Anterior segment optical coherence tomography, *AC* Anterior chamber, *ACA* Anterior chamber angle

parameters and the aqueous humor outflow. According to a recent study, Spectralis OCT with enhanced depth imaging (EDI) is able to reveal detailed optic nerve head features and different laminar and prelaminar EDI OCT-derived parameters can be obtained to characterize glaucomatous features [33]. A previous study by Spectralis OCT with EDI had identified the Schwalbe's line and scleral spur in all nasal and temporal scans [34]. In another study, by Cheung et al., using a modified Cirrus SD-OCT, the Schwalbe's line (Fig. 3.9) was identifiable in 95% of the scans and the SS was identifiable in 85% of glaucoma patients [26]. In the Casia OCT, the SS was identifiable in all study subjects. However, Schlemm's canal was only identifiable in 32% of the scans.

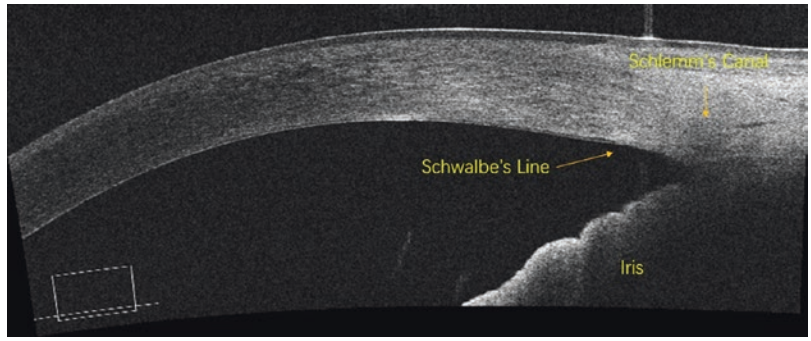

Fig. 3.9 The Schwalbe's line was identifiable in 95% of the scans and the scleral spur was identifiable in 85% of glaucoma patients

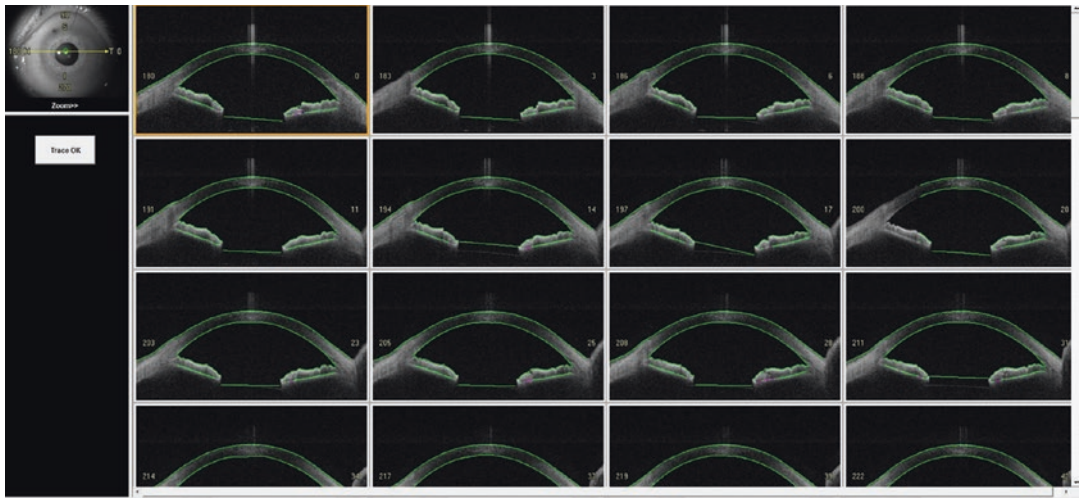

Fig. 3.10 Measurement of iris volume and anterior chamber volume with SS-OCT (This screenshot shows part of the scanning)

Its identification has also been previously reported to be subject to measurement error and variability [11, 35–37]. Accurate identification of the SS is hampered by various ocular features or conditions such as eye quadrant [31], small AC depth, narrow angle, short axial length, and older age [38]. But accurate identification of the position of the SS using AS-OCT is very important. There are many reported attempts to improve the techniques as to best identify the SS. The three most common technical approaches are (1) location of Schwalbe's line relative to the scleral spur, (2) the intersection of the ciliary muscle (CM) and the inner corneal margin, and (3) a bump-like structure in the inner corneal-meshwork margin. A study by Seager et al. demonstrated that among these three different methods, the CM approach demonstrated the highest rate of scleral spur identification with the lowest intra- and inter-observer variability [39].

Besides, the dynamic dark-light changes of the anterior chamber angle can be captured with real-time video recording and analyzed with anterior segment OCT [40]. Previous study identified that the angle width generally decreased linearly with increasing pupil diameter, and the differences of the angle width measured in the dark and in the light varied substantially among individuals [40].

3.3.2 Quantitative Metrics in 3D AS-OCT Images

The SS-OCT's low-density 3-dimensional angle analysis scan simultaneously obtains multiple

radial scans of the whole anterior chamber for the entire circumference of the angle. The instrument software automatically detected the anterior and posterior boundaries of the iris and cornea in the individual B-scans (Fig. 3.10) [41]. The iris root was defined as the intersection of the anterior and posterior iris boundaries and the ciliary body. The anterior iris boundary was detected as the anterior chamber, anterior iris surface interface, whereas the posterior iris boundary was detected as the external border of the iris pigment epithelium. The iris volume was calculated as a summation of pixel volume derived from individual B-scans [41]. In-built software analysis then analyzes the extent of iris–trabecular contact (ITC) across 360° of the angle and calculates the extent of angle-closure as the ITC index [42]. The examples of ITC index calculation were shown in Fig. 3.11. In addition, SS-OCT allows visualization and reproducible measurements of the area and degree of peripheral anterior synechia (PAS) involvement (Fig. 3.12), providing a

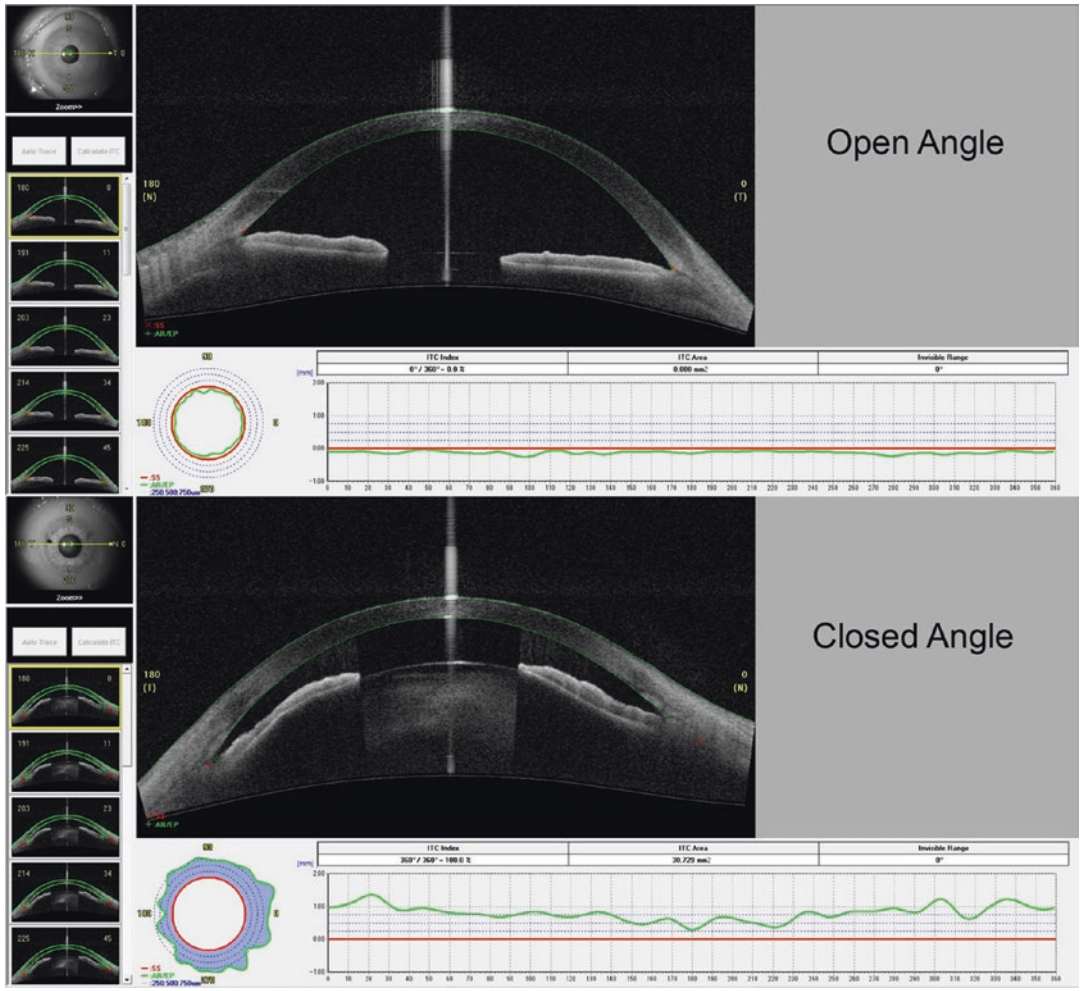

Fig. 3.11 The iridotrabecular contact (ITC) index analysis for open angle and closed angle. The "*x*" represents the scleral spur (SS) markings and the "+" represents the ITC end-point (EP). Both points are marked by an observer grading the image. The ITC chart with the blue area representing the amount and distribution of ITC. The dashed lines indicate 250 μm, 500 μm, and 750 μm from the scleral spur. The ITC graph with the *Y*-axis representing ITC (in arbitrary units) and the *X*-axis representing the degree of the angle. The graph above the red horizontal line (representing SS) demonstrates the amount of angle-closure measured as the ITC index in percentage (in red oval circle)

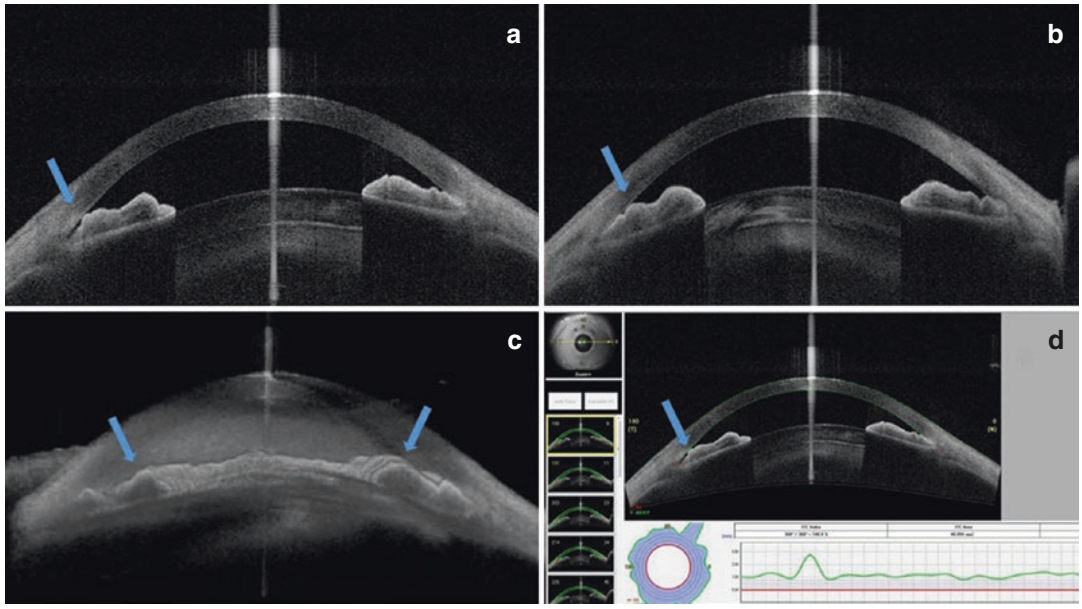

Fig. 3.12 An example showing the imaging and measurement of peripheral anterior synechia (PAS) with the swept-source optical coherence tomography (OCT) in an eye with primary angle-closure glaucoma. The horizontal (**a**) and vertical (**b**) OCT images are shown. Three-dimensional reconstruction of the OCT images reveals PAS (**c**). A polar plot of the PAS is shown in (**d**), with the red line representing the location of the scleral spur and the green line representing the location of the anterior tip of the irido-angle adhesion

new paradigm for evaluation of PAS progression and risk assessment for development of angle-closure glaucoma [43].

3.4 Conclusions

Advancements in imaging technologies and software have allowed objective and quantitative measurements of fine inner structures of the retina at high resolution. SS-OCT, with other OCT modes, efficiently and effectively detect complicated retinal features of individuals with angle closure. Computerization capabilities enable standardized procedure in collecting investigative data from individuals for objective and quantitative analysis. These current technologies can fully utilized to study a large number of individuals with angle closure, angle closure diseases such as PACG, and to follow them longitudinally to reveal their disease development [5]. Such information will provide data for biomarkers of PACG development.

Acknowledgments Prof. Clement C. Tham, Dr. Poemen Chan, and Ms. Annie Ling from the Department of Ophthalmology and Visual Sciences, The Chinese University of Hong Kong.

Compliance with Ethical Requirements Carol Y. Cheung and Yu Meng Wang declare that they have no conflict of interest. No human or animal studies were performed by the authors for this article.

References

1. Foster PJ, Buhrmann R, Quigley HA, Johnson GJ. The definition and classification of glaucoma in prevalence surveys. Br J Ophthalmol. 2002;86:238–42.
2. George R, et al. Ocular biometry in occludable angles and angle closure glaucoma: a population based survey. Br J Ophthalmol. 2003;87:399–402.
3. Liu L. Deconstructing the mechanisms of angle closure with anterior segment optical coherence tomography. Clin Exp Ophthalmol. 2011;39:614–22. https://doi.org/10.1111/j.1442-9071.2011.02521.x.
4. Wylegala E, Teper S, Nowinska AK, Milka M, Dobrowolski D. Anterior segment imaging: fourier-domain optical coherence tomography versus time-domain optical coherence tomography. J

Cataract Refract Surg. 2009;35:1410–4. https://doi.org/10.1016/j.jcrs.2009.03.034.
5. Cheung CY, et al. Factors associated with long-term intraocular pressure fluctuation in primary angle closure disease: the CUHK PACG longitudinal (CUPAL) study. J Glaucoma. 2018;27:703–10. https://doi.org/10.1097/IJG.0000000000000996.
6. Pavlin CJ, Harasiewicz K, Sherar MD, Foster FS. Clinical use of ultrasound biomicroscopy. Ophthalmology. 1991;98:287–95.
7. Pavlin CJ, Sherar MD, Foster FS. Subsurface ultrasound microscopic imaging of the intact eye. Ophthalmology. 1990;97:244–50.
8. Barkana Y, Dorairaj SK, Gerber Y, Liebmann JM, Ritch R. Agreement between gonioscopy and ultrasound biomicroscopy in detecting iridotrabecular apposition. Arch Ophthalmol. 2007;125:1331–5. https://doi.org/10.1001/archopht.125.10.1331.
9. Pavlin CJ, Harasiewicz K, Foster FS. Ultrasound biomicroscopy of anterior segment structures in normal and glaucomatous eyes. Am J Ophthalmol. 1992;113:381–9.
10. Urbak SF, Pedersen JK, Thorsen TT. Ultrasound biomicroscopy. II. Intraobserver and interobserver reproducibility of measurements. Acta Ophthalmol Scand. 1998;76:546–9.
11. Tello C, Liebmann J, Potash SD, Cohen H, Ritch R. Measurement of ultrasound biomicroscopy images: intraobserver and interobserver reliability. Invest Ophthalmol Vis Sci. 1994;35:3549–52.
12. Zhang Q, Jin W, Wang Q. Repeatability, reproducibility, and agreement of central anterior chamber depth measurements in pseudophakic and phakic eyes: optical coherence tomography versus ultrasound biomicroscopy. J Cataract Refract Surg. 2010;36:941–6. https://doi.org/10.1016/j.jcrs.2009.12.038.
13. Dada T, Sihota R, Gadia R, Aggarwal A, Mandal S, Gupta V. Comparison of anterior segment optical coherence tomography and ultrasound biomicroscopy for assessment of the anterior segment. J Cataract Refract Surg. 2007;33:837–40. https://doi.org/10.1016/j.jcrs.2007.01.021.
14. Memarzadeh F, Li Y, Chopra V, Varma R, Francis BA, Huang D. Anterior segment optical coherence tomography for imaging the anterior chamber after laser peripheral iridotomy. Am J Ophthalmol. 2007;143:877–9. https://doi.org/10.1016/j.ajo.2006.11.055.
15. Radhakrishnan S, et al. Comparison of optical coherence tomography and ultrasound biomicroscopy for detection of narrow anterior chamber angles. Arch Ophthalmol. 2005;123:1053–9. https://doi.org/10.1001/archopht.123.8.1053.
16. Radhakrishnan S, Rollins AM, Roth JE, Yazdanfar S, Westphal V, Bardenstein DS, Izatt JA. Real-time optical coherence tomography of the anterior segment at 1310 nm. Arch Ophthalmol. 2001;119:1179–85.
17. Shabana N, et al. Quantitative evaluation of anterior chamber parameters using anterior segment optical coherence tomography in primary angle closure mechanisms. Clin Exp Ophthalmol. 2012;40:792–801. https://doi.org/10.1111/j.1442-9071.2012.02805.x.
18. Sng CC, et al. Determinants of anterior chamber depth: the Singapore Chinese eye study. Ophthalmology. 2012;119:1143–50. https://doi.org/10.1016/j.ophtha.2012.01.011.
19. Li P, Johnstone M, Wang RK. Full anterior segment biometry with extended imaging range spectral domain optical coherence tomography at 1340 nm. J Biomed Opt. 2014;19:046013. https://doi.org/10.1117/1.JBO.19.4.046013.
20. Nongpiur ME, et al. Lens vault, thickness, and position in Chinese subjects with angle closure. Ophthalmology. 2011;118:474–9. https://doi.org/10.1016/j.ophtha.2010.07.025.
21. Nongpiur ME, et al. Novel association of smaller anterior chamber width with angle closure in Singaporeans. Ophthalmology. 2010;117:1967–73. https://doi.org/10.1016/j.ophtha.2010.02.007.
22. Moghimi S, et al. Ocular biometry in the subtypes of angle closure: an anterior segment optical coherence tomography study. Am J Ophthalmol. 2013;155:664–673, 673 e661. https://doi.org/10.1016/j.ajo.2012.10.014.
23. Ramos JL, Li Y, Huang D. Clinical and research applications of anterior segment optical coherence tomography – a review. Clin Exp Ophthalmol. 2009;37:81–9. https://doi.org/10.1111/j.1442-9071.2008.01823.x.
24. Rodrigues EB, Johanson M, Penha FM. Anterior segment tomography with the cirrus optical coherence tomography. J Ophthalmol. 2012;2012:806989. https://doi.org/10.1155/2012/806989.
25. Xu BY, Mai DD, Penteado RC, Saunders L, Weinreb RN. Reproducibility and agreement of anterior segment parameter measurements obtained using the CASIA2 and Spectralis OCT2 optical coherence tomography devices. J Glaucoma. 2017;26:974–9. https://doi.org/10.1097/IJG.0000000000000788.
26. Cheung CY, et al. Novel anterior-chamber angle measurements by high-definition optical coherence tomography using the Schwalbe line as the landmark. Br J Ophthalmol. 2011;95:955–9. https://doi.org/10.1136/bjo.2010.189217.
27. Kagemann L, et al. Identification and assessment of Schlemm's canal by spectral-domain optical coherence tomography. Invest Ophthalmol Vis Sci. 2010;51:4054–9. https://doi.org/10.1167/iovs.09-4559.
28. Fukuda S, Kawana K, Yasuno Y, Oshika T. Repeatability and reproducibility of anterior chamber volume measurements using 3-dimensional corneal and anterior segment optical coherence tomography. J Cataract Refract Surg. 2011;37:461–8. https://doi.org/10.1016/j.jcrs.2010.08.053.
29. Ishikawa H, Esaki K, Liebmann JM, Uji Y, Ritch R. Ultrasound biomicroscopy dark room provocative testing: a quantitative method for estimating anterior chamber angle width. Jpn J Ophthalmol. 1999;43:526–34.

30. Sung KR, Lee KS, Hong JW. Baseline anterior segment parameters associated with the long-term outcome of laser peripheral Iridotomy. Curr Eye Res. 2015;40:1128–33. https://doi.org/10.3109/02713683.2014.986334.
31. Sakata LM, Lavanya R, Friedman DS, Aung HT, Seah SK, Foster PJ, Aung T. Assessment of the scleral spur in anterior segment optical coherence tomography images. Arch Ophthalmol. 2008b;126:181–5. https://doi.org/10.1001/archophthalmol.2007.46.
32. Wang BS, et al. Increased iris thickness and association with primary angle closure glaucoma. Br J Ophthalmol. 2011;95:46–50. https://doi.org/10.1136/bjo.2009.178129.
33. Lopes FS, Matsubara I, Almeida I, Dorairaj SK, Vessani RM, Paranhos A Jr, Prata TS. Structure-function relationships in glaucoma using enhanced depth imaging optical coherence tomography-derived parameters: a cross-sectional observational study. BMC Ophthalmol. 2019;19:52. https://doi.org/10.1186/s12886-019-1054-9.
34. Day AC, et al. Spectral domain optical coherence tomography imaging of the aqueous outflow structures in normal participants of the EPIC-Norfolk eye study. Br J Ophthalmol. 2013;97:189–95. https://doi.org/10.1136/bjophthalmol-2012-302147.
35. Leung CK, et al. Novel approach for anterior chamber angle analysis: anterior chamber angle detection with edge measurement and identification algorithm (ACADEMIA). Arch Ophthalmol. 2006;124:1395–401. https://doi.org/10.1001/archopht.124.10.1395.
36. Li H, Leung CK, Cheung CY, Wong L, Pang CP, Weinreb RN, Lam DS. Repeatability and reproducibility of anterior chamber angle measurement with anterior segment optical coherence tomography. Br J Ophthalmol. 2007;91:1490–2. https://doi.org/10.1136/bjo.2007.118901.
37. Sakata LM, et al. Comparison of gonioscopy and anterior segment ocular coherence tomography in detecting angle closure in different quadrants of the anterior chamber angle. Ophthalmology. 2008a;115:769–74. https://doi.org/10.1016/j.ophtha.2007.06.030.
38. Liu S, et al. Assessment of scleral spur visibility with anterior segment optical coherence tomography. J Glaucoma. 2010;19:132–5. https://doi.org/10.1097/IJG.0b013e3181a98ce4.
39. Seager FE, Wang J, Arora KS, Quigley HA. The effect of scleral spur identification methods on structural measurements by anterior segment optical coherence tomography. J Glaucoma. 2014;23:e29–38. https://doi.org/10.1097/IJG.0b013e31829e55ae.
40. Leung CK, et al. Dynamic analysis of dark-light changes of the anterior chamber angle with anterior segment OCT. Invest Ophthalmol Vis Sci. 2007;48:4116–22. https://doi.org/10.1167/iovs.07-0010.
41. Mak H, Xu G, Leung CK. Imaging the iris with swept-source optical coherence tomography: relationship between iris volume and primary angle closure. Ophthalmology. 2013;120:2517–24. https://doi.org/10.1016/j.ophtha.2013.05.009.
42. Baskaran M, Ho SW, Tun TA, How AC, Perera SA, Friedman DS, Aung T. Assessment of circumferential angle-closure by the iris-trabecular contact index with swept-source optical coherence tomography. Ophthalmology. 2013;120:2226–31. https://doi.org/10.1016/j.ophtha.2013.04.020.
43. Lai I, Mak H, Lai G, Yu M, Lam DS, Leung CK. Anterior chamber angle imaging with swept-source optical coherence tomography: measuring peripheral anterior synechia in glaucoma. Ophthalmology. 2013;120:1144–9. https://doi.org/10.1016/j.ophtha.2012.12.006.